Estuaries and Coasts (2009) 32:100–110
DOI 10.1007/s12237-008-9109-9

ORIGINAL PAPER

Thermal Variability in a Tidal River

Stephen G. Monismith · James L. Hench · Derek A. Fong · Nicholas J. Nidzieko · William E. Fleenor · Laura P. Doyle · S. Geoffrey Schladow

Received: 14 February 2008 / Revised: 10 September 2008 / Accepted: 6 October 2008 / Published online: 29 October 2008
© Coastal and Estuarine Research Federation 2008

Abstract In this paper, we discuss observations of temperature variability in the tidal portion of the San Joaquin River in California. The San Joaquin River makes up the southern portion of the Sacramento San Joaquin Delta, the eastern end of San Francisco Bay. Observations made in August 2004 and August 2005 show significant diurnal variations in temperature in response to surface heat exchange. However, to account for observed changes in heat content a sizeable downstream heat flux (approximately 100 W m^{-2}) must be added to the surface heat flux. To account for this flux via Fickian dispersion, a flow-dependent dispersion coefficient varying from 500 to 4,000 m^2 s^{-1} is needed. These values are much larger than would be predicted for a river of this size, suggesting that the complex topology of the Delta greatly enhances longitudinal dispersion. Building on these observations, we present a simple theory that explores how the subtidal temperature field varies in response to changes in flow rate, dispersion, and heat exchange.

Keywords Estuaries · Tides · Water temperature · Dispersion · Surface heat exchange

S. G. Monismith (✉) · J. L. Hench · D. A. Fong · N. J. Nidzieko
Environmental Fluid Mechanics Laboratory, Stanford University, Stanford, CA 94305-4020, USA
e-mail: monismith@stanford.edu

W. E. Fleenor · L. P. Doyle · S. G. Schladow
Department of Civil and Environmental Engineering, University of California, Davis, CA 95616, USA

Introduction

Models to predict temperatures in rivers and lakes are in common use (see e.g., Bohrmans and Webster 1998). For example, models of river and stream temperatures have been used to develop standards for waste heat discharge, to design reservoir release strategies, and to understand annual variations in a variety of biogeochemical processes such as nutrient cycling or the development of harmful algal blooms. In lakes, variability in temperature stratification plays a central role in mixing and transport, thus determining the rates and paths by which different portions of the lake are connected to each other (Romero et al. 2004).

Predictions of temperatures in estuaries are less commonly reported (see Uncles and Stephens 2001 for a notable exception), at least partially, because temperature is generally assumed to have little effect on flow dynamics in most estuaries. Nonetheless, in many cases, knowledge of temperature is important because it is important biologically. For example, in the complex of interconnected channels where the Sacramento and San Joaquin rivers come together (hereinafter referred to as "the Delta"), water temperature standards have been developed to protect outmigrating chinook salmon smolts. Additionally, it is known that temperature strongly influences when Delta Smelt, an endangered native fish resident in the Delta, spawn (Bennett 2005). Predictions of water temperatures are thus important to understanding when spawning will take place and thus when larval Delta Smelt are likely to be present in the system, information that is important in operating in-Delta diversions so as to minimize entrainment losses (Bennett 2005).

In this paper, we report observations of temperature variation gathered as part of a project studying the effects of thermal stratification on low dissolved oxygen in the Deep

Water Ship Channel (DWSC) of the San Joaquin River (SJR). The original motivation for this work was the hypothesis that stratification played an important role in the development of hypoxia in this system (Jassby 2005; Jassby and Van Nieuwenhuyse 2005).

Overall, the variation in temperature can be described by the Reynolds averaged heat conservation equation (see e.g., Tennekes and Lumley 1972),

$$\frac{\partial \overline{\theta}}{\partial t} + \overline{U} \cdot \nabla \overline{\theta} \cong -\frac{\partial}{\partial z}\left(\overline{w'\theta'}\right) \tag{1}$$

where $\overline{\theta}$ and $\overline{U}$ are the tidally varying Reynolds averaged temperature and velocities, θ' and w' are the turbulent fluctuating temperature and vertical velocity, and z is vertical position.

If Eq. 1 is integrated over the cross-sectional area and is filtered to remove tidal variations, a one-dimensional advection diffusion equation results (see e.g., Edinger et al. 1974; Fischer et al. 1979; Uncles and Stephens 2001)

$$A(x)\frac{\partial T}{\partial t} - Q_f \frac{\partial T}{\partial x} = \frac{\partial}{\partial x}\left(K(x)A(x)\frac{\partial T}{\partial x}\right) - \frac{WH_f}{\rho c_p} \tag{2}$$

In this equation, A is the cross-sectional area, Q_f is the river flow, T is the cross-sectionally averaged and subtidally filtered temperature, K is the dispersion coefficient, W is the local width, and H_f is the surface heat flux in W m^2. The usual sign convention is that H_f is negative for heating of the water column and positive for cooling. (see Fig. 1). The x-axis points upstream. Such 1D models have a long history in the theory and modeling of salinity in estuaries (see e.g., Savenije 2005; Monismith et al. 2002). As discussed in Fischer (1976), the sub-tidal representation of tidally averaged sheared advection is usually assumed to take the form of Fickian diffusion, although as discussed by Ridderinkhof and Zimmerman (1992), such advection need not lead to pure Fickian diffusion, instead, depending on the mechanism causing the shear, can lead to scale-dependent dispersion.

In this paper, we discuss what shapes the along-channel variation of temperature observed in the tidal San Joaquin River, emphasizing how the processes described in Eq. 2, namely advection, surface heat fluxes, and most notably, dispersion, all play an important roles in determining the temperature field we observe.

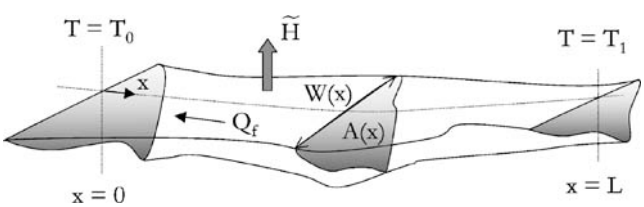

Fig. 1 Sketch of tidal river for one-dimensional analysis

Field Site and Data Collection

The San Joaquin River flows west from the Sierra Nevada mountains into the southern San Joaquin valley and then north into the Delta formed by the confluence of the San Joaquin and Sacramento Rivers. The Delta itself consists of a matrix of hundreds of levee-bordered islands of different sizes created in the nineteenth century by "reclamation" of the tidal marsh through which the Sacramento and San Joaquin Rivers flowed in San Francisco Bay. For approximately 30 km starting near the city of Stockton, the San Joaquin has been dredged to create the Deep Water Ship Channel, a channel that facilitates passage of shipping to the port of Stockton (Fig. 2). Near the junction of the San Joaquin River with the DWSC, there is a dead-end section of channel used for turning around ships visiting the port. Except for peak runoff events, most of the natural flow in the river is diverted for use by irrigated agriculture, such that in summer, non-tidal flows of freshwater into the Delta might only amount to O(10) m^3 s^{-1}. Tidal flows in the Delta are stronger, with tidal velocities in the DWSC ranging from 0.1 to 0.3 m s^{-1}, with stronger velocities found at seaward end of the river. Nonetheless, the flows remain primarily tidal until at least 20 km upstream of the start of the DWSC. In this portion of the Delta, salinities are close to zero and are not dynamically significant. For further information, the reader is referred to Jassby (2005).

In August 2004 and 2005, we deployed, for several weeks at a time, a series of moorings including temperature loggers and current meters at a series of stations arranged as shown in Fig. 1. Our set of temperature loggers included Richard Brancker Research TR1000, Oregon Environmental 9311, and Seabird 39 units. When newly calibrated, these all have accuracies approaching 0.002°C, although for our data sets, comparison of data from instruments of different types and ages on the same mooring suggested typical calibration offsets of as much as 0.2°C. Velocity measurements were made using 1,200 kHz RD Instruments workhorse ADCPs, deployed on the bottom looking up through the water column and measuring velocities from about 0.6 mab (meters above bottom) and covering about 90% of the total water column depth in 0.25-m bins.

In addition to our instruments, we also obtained other data from several local, state, and federal agencies, notably flow in the San Joaquin River measured ultrasonically by the USGS approximately 4 km upstream of the junction of the DWSC and the SJR, and temperatures measured by the California Dept of Water Resources[1] at various stations along the SJR both upstream and downstream of our moorings.

[1] http://cdec.water.ca.gov/

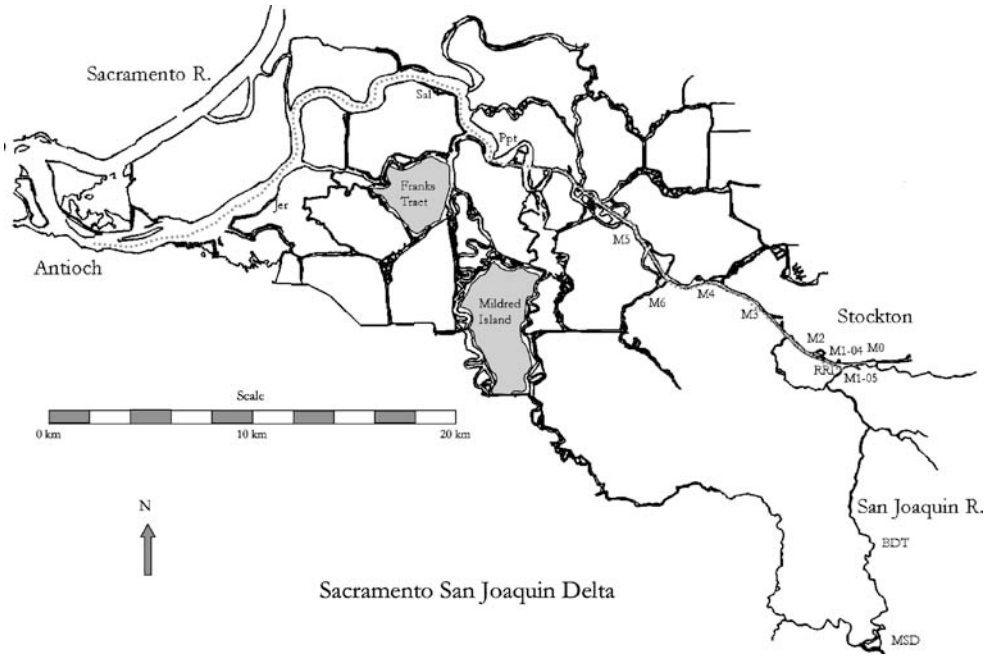

Fig. 2 Overview of the Sacramento San Joaquin Delta. Along with instrument locations for 2004 and 2005 experiments (*M0 to M6*), positions of selected California Dept. of Water Resources continuous monitoring (e.g., *MSD* Mossdale) stations are also shown. One DWR station on the San Joaquin River, Vernalis (VER), is not shown; it is approximately 45 km south of MSD

As discussed in detail in Edinger et al. (1974) (see also Pawlowicz et al. 2001), heat fluxes through the air–water interface are due to shortwave radiation (Q_w), net longwave radiation (Q_{lw}), latent heat transfer (H_l), and sensible heat transfer (H_s). The total surface heat exchange can be written as

$$H_f = Q_{sw} + Q_{lw} + H_l + H_s \quad (3)$$

The first term on the right of Eq. 3 is usually measured, whereas the other three terms are computed using empirical formulae based on measured surface water temperature, air temperature, relative humidity and wind speed, and cloud cover (see Fischer et al. 1979).

Meteorological data were obtained from the Port of Stockton (wind speed and direction, air temperature ,and relative humidity) and for the CIMIS[2] weather station in Manteca (incident shortwave radiation), closest to, but approximately 20 km NNW from our M2 mooring. Examination of other CIMIS stations in this part of California (e.g., one 20 km WSW of Manetca) showed a high degree of correlation ($R^2 \approx 0.99$) with nearly identical shortwave radiation values such that mean shortwave radiation values were different by less than 8 W/m^2. Combined with our surface temperature data, these sets of meteorological data were used to compute heat fluxes (latent, sensible, and net longwave) using the set of Matlab™ routines describe by Palowiscz et al. (2001). Because we did not have any data on cloud fraction, i.e., the portion of the sky covered by clouds, we assumed a "cloudiness" of 0.9 (cloudiness=1 corresponds to a clear sky) of for all our calculations. Exploration of diurnal stratification dynamics using the 3D circulation model Si3D (Rueda and Schladow 2003) and the 2004 data set suggested that the measured shortwave radiation should be reduced by 10% and that latent and sensible heat fluxes should be increased by 10% to best model the stratification that developed diurnally. The albedo chosen is the same as what Cole et al. (1992) used to model photosynthesis in the tidal freshwater region of the Hudson estuary, and is within the range of values given by Mohseni and Stefan (1999). These increases in surface heat exchanges are reasonable given uncertainty in the applicability of bulk meteorological formulae developed for open ocean conditions to limited fetch waterbodies like the DWSC and the extent to which winds measured at the Port of Stockton represent winds over the domain of interest. These changes were used for both the 2004 and 2005 data sets.

Observations

Tides, depth-averaged velocities, heat fluxes, and depth-averaged temperatures for August 2004 for our mooring stations are shown in Fig. 3. As observed, diurnal variations dominate variations in temperature, with little direct effect of tides. These diurnal variations included diurnally varying vertical stratification of 2 to 4°C that developed through the day due to heating and broke down at night due to cooling. Results from our study pertaining to stratification dynamics will be reported elsewhere.

Spatial variations in temperature are also clear, with the warmest temperatures generally seen at the upstream end of

[2] http://wwwcimis.water.ca.gov/cimis/

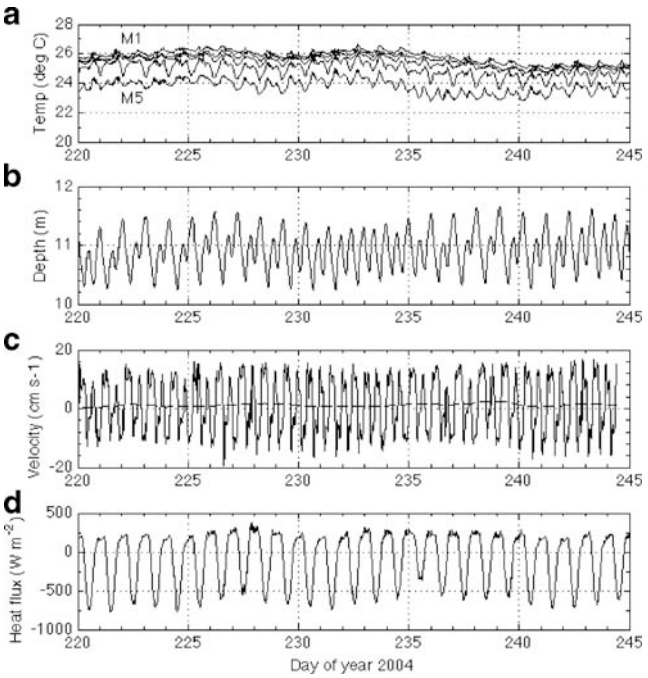

Fig. 3 **a** Temperature; **b** depth at M2; **c** depth-averaged velocities at M2; and **d** heat fluxes; all for August 2004

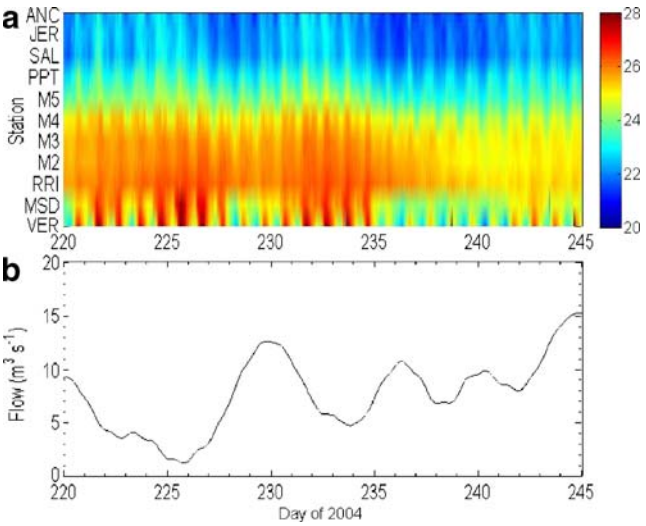

Fig. 4 San Joaquin River July/Aug 2004: **a** Temperatures—Stations are Vernalis (*VER*), Mossdale (*MSD*), Brandt bridge (*BDT*), M0, Rough and Ready Island (*RRI*), M1, M2, M5, Prisoners Point (*PPT*), San Andreas Landing (*SAL*), Jersey point (*JER*), and Antioch (*ANC*). All are given in °C; **b** subtidal flows measured upstream of the DWSC

the DWSC (M1) and the coldest at the downstream end (M3). The small tidal variation in temperature can be explained by noting that the temperature change over one tidal cycle due to advection by a sinusoidally varying tidal velocity is

$$\Delta T_{\text{tidal}} \approx \frac{U_{\text{tide}}}{\omega_{\text{tide}}} \frac{\partial T}{\partial x} \tag{4}$$

where U_{tide} is the peak velocity of tide with frequency ω_{tide}. For the DWSC, $U_{\text{tide}} \approx 0.1$ m/s, $\omega_{\text{tide}} \approx 1.5 \times 10^{-4}\ s^{-1}$, and $\partial T/\partial x \approx 10^{-4}$°C s^{-1}. Thus, $\Delta T_{\text{tidal}} \approx 0.1$°C, in contrast with diurnal variations of approximately 1°C. Note that subtidal variations in the longitudinal temperature gradient mean that harmonic analysis of temporal temperature variations would not be especially useful.

The combination of spatial and temporal variations in temperature for the entire San Joaquin system (river to estuary) are shown for 2004 (Fig. 4) and 2005 (Fig. 5), with the *x*-axis in each image representing time and the *y*-axis in the upper panel of each figure showing stations, arrayed with downstream (Antioch) at the top of the figure and upstream (Vernalis) at the bottom. In addition to diurnal variations, both 2004 and 2005 show significant longer period variations that may either be associated with changes in meteorological forcing (especially the latter half of 2005, which was a period of significant cooling) or in spring-neap variations in upstream (negative) heat flux.

Interestingly, the 2004 data show two different temperature patterns, one in which the temperatures monotonically increase up into the river and one in which the DWSC near Stockton [i.e., near Rough and Ready Island (RRI)] is the warmest part of the San Joaquin. The 2005 data only show the latter pattern, a likely effect of larger flows in August 2005 than in August 2004 (Fig. 5b). Nonetheless, the overall mean spatial structure of the temperature field for both years are (Figs. 6 and 7) similar. Most importantly, both data sets show the importance of heat fluxes from both the Bay and from the San Joaquin River in setting temperatures in the DWSC. For example, at a tidally

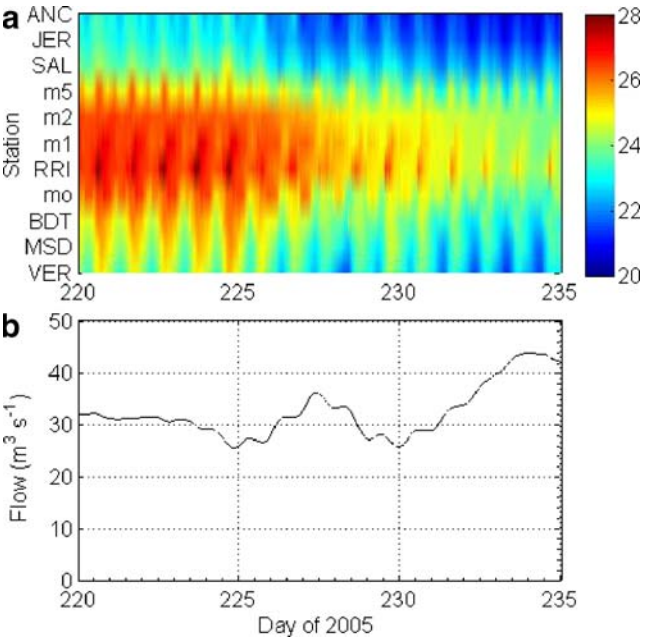

Fig. 5 Same as Fig. 4 except for July/Aug 2005. Labels as above

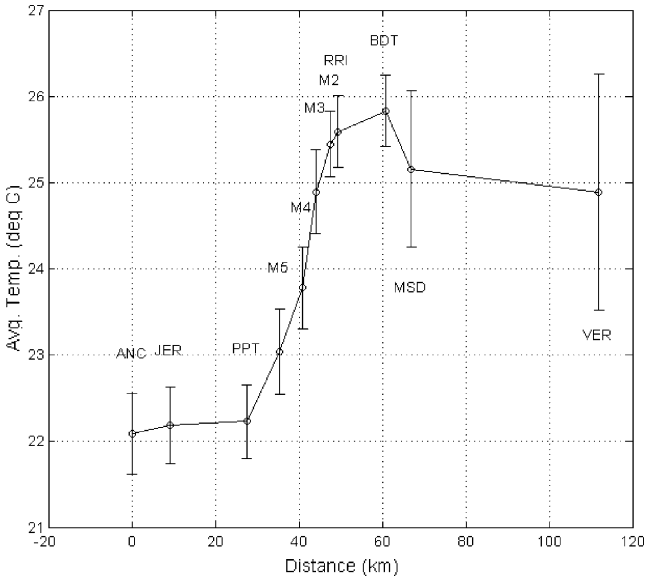

Fig. 6 Spatial variations in temperature August 2004. Mean values are average over entire record from experiment. *Error bars* show standard deviations of temperature at each station. Labels as in Figs. 4 and 5

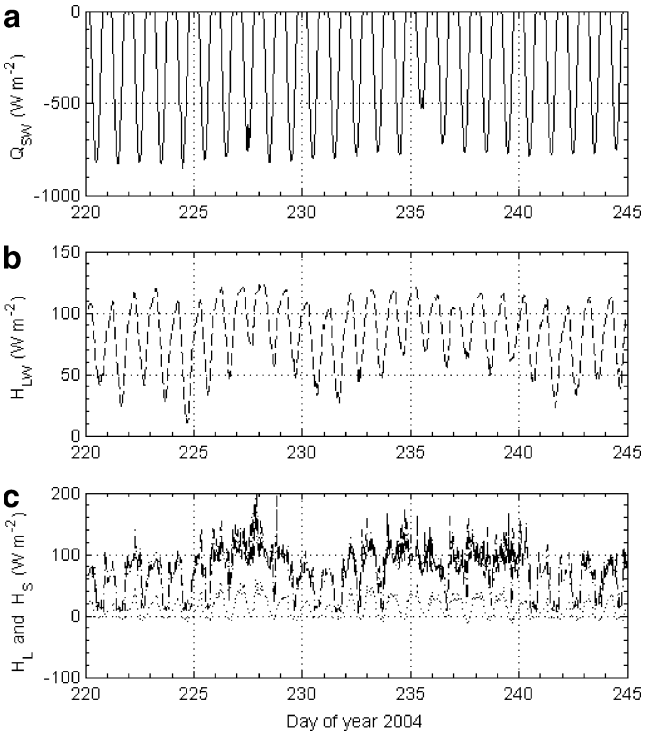

Fig. 8 Heat fluxes for 2004: **a** shortwave radiation; **b** longwave radiation; (c) latent (*solid line*) and sensible (*broken line*) heat flux

averaged flow of 20 m^3 s^{-1} (600 cfs), the 3°C drop in temperature between M0 and M5 is equivalent to approximately 100 W m^{-2} surface heat flux, i.e., is comparable to significant rates of heating or cooling due to synoptic weather variability.

The calculated fluxes for 2004 are shown in Fig. 8, where it can be seen that latent heat fluxes make up a significant fraction of the overall thermal energy balance. The data from 2005 are similar and are not shown. To assess the fidelity of this heat flux, we compared the cumulative change in heat content with the change in thermal energy content at the M2 mooring for both 2004 and 2005 (Fig. 9); i.e., integrating (1) with respect to depth

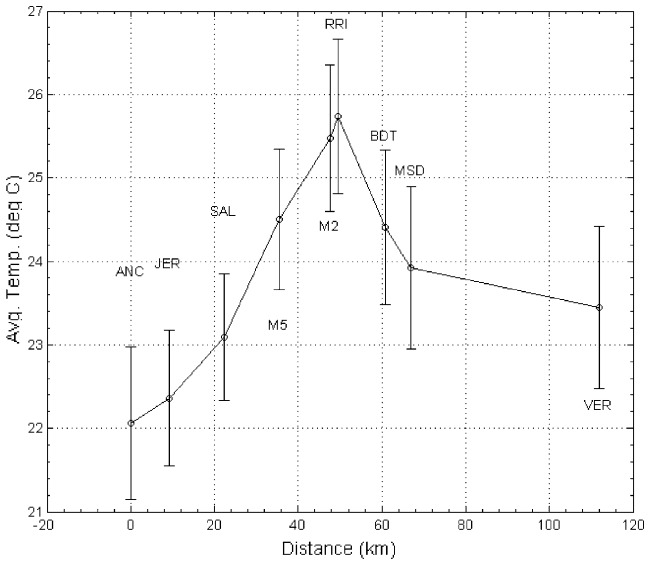

Fig. 7 Spatial variations in temperature, August 2005. Mean values are average over entire record from experiment. *Error bars* show standard deviations of temperature at each station. Labels as in Figs. 4 and 5

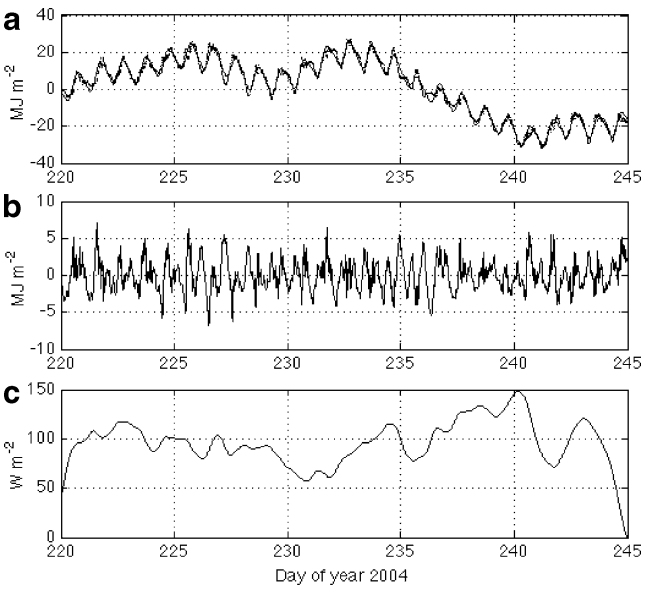

Fig. 9 **a** Observed (*dotted line*) and computed (*solid line*) heat content variation; **b** difference between observed and computed heat content; **c** subtidal correction heat flux. The zeroes at the ends of the records in **c** are an artifact of the filtering

and neglect advection, the rate of change of heat content due to surface fluxes is

$$\rho c_p \frac{d}{dt} \int_{-D}^{0} \overline{\theta}\, dz = -H_s \tag{5}$$

where D is the local depth. In both cases, the computed fluxes show net heating, whereas the observations in general do not. There is also a tidal variation that spectral analysis (not shown) revealed is primarily semidiurnal, although other periods (24, 8, 6, 4.8, and 4 h) are also present. These frequencies reflect the spectral energy content of the velocity record shown in Fig. 3c.

For 2004, the imbalance amounts to an average heat loss of over 100 W m^{-2}, a number that is far larger than potential errors in computing the heat flux. For example, uncertainty in the net longwave radiation due to uncertainty about cloud cover and uncertainty in shortwave radiation due to uncertainty in albedo are each less than 10 W/m^2. This imbalance can be used to estimate the net horizontal heat transport as the subtidal difference between the rate of change of heat content and the incoming heat fluxes. Calculating this way (Fig. 9c) reveals a downriver heat flux of approximately 50 to 150 W/m^2, with the sign of the flux correct for Fickian diffusion-like process.

We can evaluate the relative importance of subtidal advection and dispersion by integrating Eq. 2 from $x=x_0$, the downstream end of DWSC to the upstream end at Stockton, $x=x_1$ and assuming that the surface heat flux is uniform (in the absence of any other data). This gives

$$\rho c_p \overline{D} \frac{\partial \overline{T}}{\partial t} + H_f \approx -\frac{\rho c_p K(x_0) A(x_0) \frac{\partial T}{\partial x}(x_0)}{\overline{W}(x_1 - x_0)} + \rho c_p Q_f \frac{(T(x_1) - T(x_0))}{\overline{W}(x_1 - x_0)} \tag{6}$$

where quantities with overbars are averages between $x=x_0$ and $x=x_1$, so that K can be determined from the heat balance. To carry out this calculation, the heat content, flows, etc. were low-pass filtered using a fourth order Butterworth filter with a cutoff frequency of 0.25 cpd. Based on the data shown in Figs. 6 and 7, $\partial T/\partial x$ was calculated from the difference in temperature between M2 and Prisoner Point (PPT) for 2004, whereas for 2005, we used RRI and Antioch.

The results of this calculation for the 2004 data are shown in Fig. 10, where it can be seen that values of K range from 500 to 900 m^2 s^{-1}. The same calculation for 2005 is shown in Fig. 11, where even larger values of K (up to 4000 m^2 s^{-1}) are evident. Note that since these values of K come from a requirement to lose heat from the DWSC, they cannot be an effect of error in the measured flow rate, since the overall contribution to the needed heat flux is small and has the wrong sign. Somewhat surprisingly,

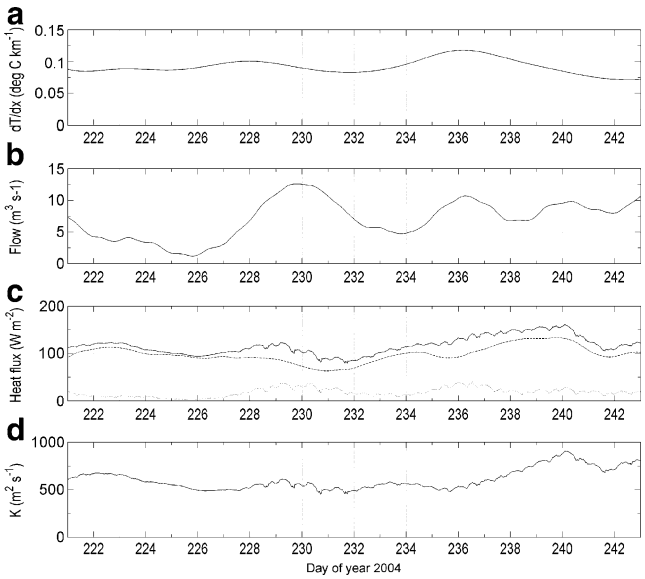

Fig. 10 Inferred dispersion coefficients from heat balance for 2004: **a** horizontal temperature gradient; **b** subtidal flow in San Joaquin River; **c** advective heat flux (*dotted line*), inferred correction to 1D balance (*broken line*), and total dispersive heat flux (*solid line*); **d** inferred longitudinal dispersion coefficient

combining the two data sets (Fig. 12) reveals a substantial and unexpected dependence on flow.

These values of K are at the large end of what is typically found for rivers and estuaries (see Fischer et al. 1979). For example, the dispersion coefficient associated with an oscillating shear flow can be approximated by

$$K \approx 0.2 \frac{W^2 U^2}{D u_*} f\left(\frac{\omega W^2}{D u_*}\right) \tag{7}$$

where u_* is the average shear velocity and the function f is given in Fischer et al. (1979). Using values of W, etc., appropriate to the DWSC, we find that a value of $K \approx 30$ m^2 s^{-1} would be predicted.

Thus, it seems likely that the large value of K required for the thermal energy balance reflects the dispersive effects of the numerous channel junctions and bifurcations along the SJR. Indeed, 2D calculations by Monsen (2001) showed that in-channel sub-tidal fluxes of scalars are largely due to advection. Thus, the observed dispersion must be associated almost exclusively with the channel junctions. The dependence on mean flow may be associated with an increase in the tendency for fluid particles in the DWSC to "sample" several geometrically complex features, e.g., the divided channels near M5.

From the practical standpoint of predicting temperatures in a complex system like the tidal San Joaquin River, the fact that subtidal dispersive heat fluxes are comparable to net surface heat exchanges means that hydrodynamic

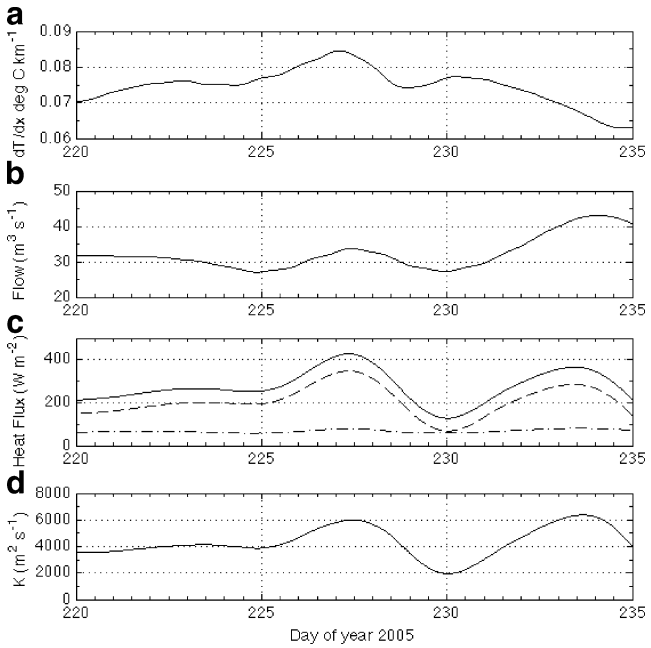

Fig. 11 Inferred dispersion coefficients from heat balance for 2005: **a** Horizontal temperature gradient; **b** subtidal flow in San Joaquin River; **c** advective heat flux (*dotted line*), inferred correction to 1D balance (*broken line*), and total dispersive heat flux (*solid line*); **d** inferred longitudinal dispersion coefficient

models like that used by Monsen (2001) or DeGeorge (1996) must do a reasonable job at predicting dispersive heat fluxes and making use of accurate surface heat fluxes if it is to accurately predict temperature. In the next section, we discuss, in an idealized fashion, this balance of dispersion and surface heating.

Theory

We focus in this paper on a simple analytical model of subtidal variations in temperature. Consequently, we also assume the heat flux to be constant or at least not vary diurnally. We also assume that the temperature is, to first order, uniform across the cross-section and thus varies only in the longitudinal direction. Thus, our starting point is the 1D advection dispersion equation for heat, including surface heating through an imposed surface heat that depends on wind speed, air-water temperature difference, etc. given above.

For the sake of developing analytical solutions that describe the main features of the temperature distributions reported above, we further neglect time variations, assume that K and A do not depend on x, and that the surface heat exchange can be represented by the form

$$\frac{H_f}{\rho c_p} = -\alpha(T_e - T) \tag{8}$$

where α is the heat transfer velocity and T_e is the equilibrium temperature in the water, both of which are functions of the given the meteorological conditions and the incident shortwave radiation (Mohseni and Stefan 1999). With these drastic simplifications, it becomes

$$-\frac{Q_f}{A}\frac{\partial T}{\partial x} = K\frac{\partial^2 T}{\partial x^2} + \alpha\frac{(T_e - T)}{D} \tag{9}$$

where $D=A/W$ is the effective depth. We suppose that the temperature at the riverine and ocean ends of this tidal river are specified. Without loss of generality, these can be assumed to be the same, so that

$$T = T_0 \quad x = 0, L \tag{10}$$

To proceed, we look at the deviation of the temperature from T_0, i.e.

$$T' = T - T_0 \tag{11}$$

and then construct dimensionless variables from the temperature difference $\Delta T = T_e - T_0$:

$$\begin{aligned} T^* &= T'/\Delta T \\ x^* &= x/L \end{aligned} \tag{12}$$

In terms of these dimensionless variables, Eq. 9 becomes

$$\frac{\partial^2 T^*}{\partial x^{*}{}_2} + \frac{Q_f L}{KA}\frac{\partial T^*}{\partial x^*} = -\frac{\alpha L^2}{KD}\left(1 - T^*\right) \tag{13}$$

or

$$\frac{\partial^2 T^*}{\partial x^{*}{}_2} + P_1\frac{\partial T^*}{\partial x^*} = -P_2\left(1 - T^*\right) \tag{14}$$

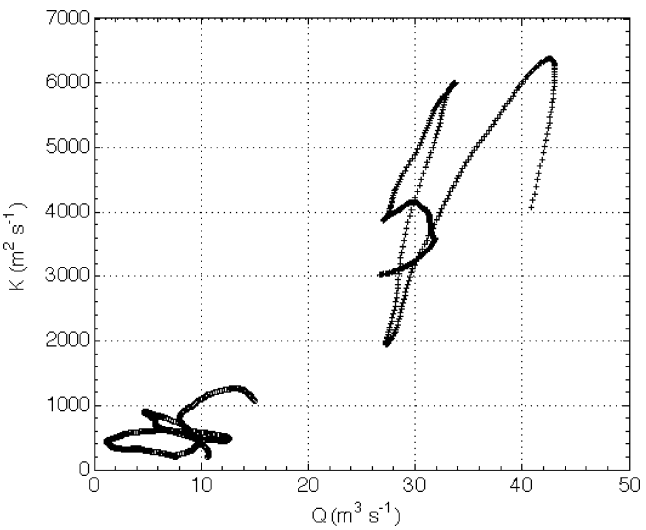

Fig. 12 Inferred dispersion coefficients as a function of flow for 2004 (*circle*) and 2005 (*plus*)

The parameter $P_1=Q_fL/KA$ reflects the relative importance of advection and dispersion; this term will be important when L is comparable to or larger than intrusion length KA/Q_f that plays a fundamental role in salinity intrusion when salinity variations are present (which is not the case in the DWSC). $P_2=\alpha L^2/KD$ reflects the relative importance of diffusion to heat exchange. In this case, heat transfer will be important when L is comparable to or larger than the diffusion scale $(KD/\alpha)^{1/2}$.

The solution to Eq. 14, given the imposed conditions, is easily found to be

$$T^* = 1 + A_+ \exp\left(\lambda_+ x^*\right) + A_- \exp\left(\lambda_- x^*\right) \tag{15}$$

where

$$\lambda_\pm = -\frac{P_1}{2} \pm \frac{\sqrt{P_1^2 + 4P_2}}{2}$$

$$A_+ = \frac{-1 + \exp(\lambda_-)}{\exp(\lambda_+)} \left(1 - \frac{\exp(\lambda_-)}{\exp(\lambda_+)}\right)^{-1}$$

$$A_- = -1 - A_+$$

As expected, the nature of the temperature field in the river depends on both advection and heat exchange, i.e., for systems like the San Joaquin River, on both water project operations (which determine flows in summer) and on weather. The solution given by Eq. 15 can easily be modified to choose $T^*(1)=\delta$, i.e., to specify an upstream temperature that is $T_0+\delta\Delta T$. For this case, A_- remains as given above (in terms of A_+) but A_+ becomes

$$A_+ = \frac{\delta - 1 + \exp(\lambda_-)}{\exp(\lambda_+) - \exp(\lambda_-)} \tag{16}$$

In Figs. 13 and 14, we have plotted sample solutions for different values of P_1 and P_2. The basic behavior that emerges is that for weak flows, the temperature approaches the equilibrium temperature, whereas for strong flows, the temperature remains close to that of the boundaries, in all cases, because the maximum temperature is found in the interior of the domain, exactly as seen in the observations. This simple theory shows that as the flow rate drops, upstream diffusion of "coldness" from the downstream boundary becomes increasingly important. For the case with asymmetrical boundary conditions, as the flow (Fig. 15) increases, the maximum temperature in the interior rises as the flow carries heat from the upstream boundary further into the domain.

For the case of an asymmetrical temperature distributions, the effects of the upstream boundary condition seem to be stronger than the direct effects of flow (Fig. 16). However, the inflow temperature itself is also an effect of flow in that the water that enters the tidal portion of the system often comes from an upstream reservoir that is

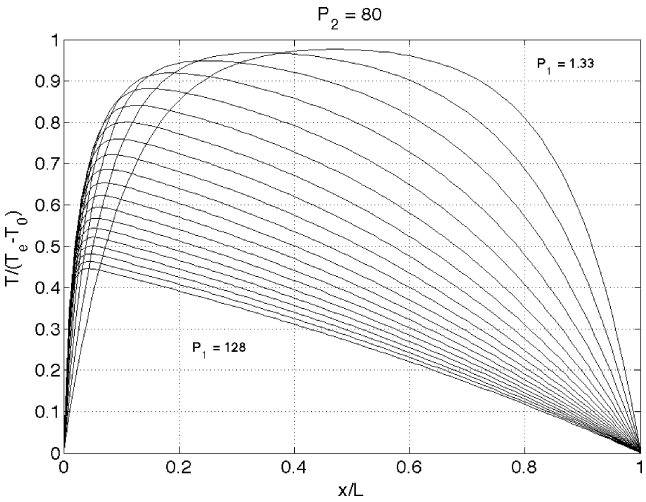

Fig. 14 Dimensionless temperature as computed by theory for $P_2=80$ and $1.33\leq P_1\leq 128$

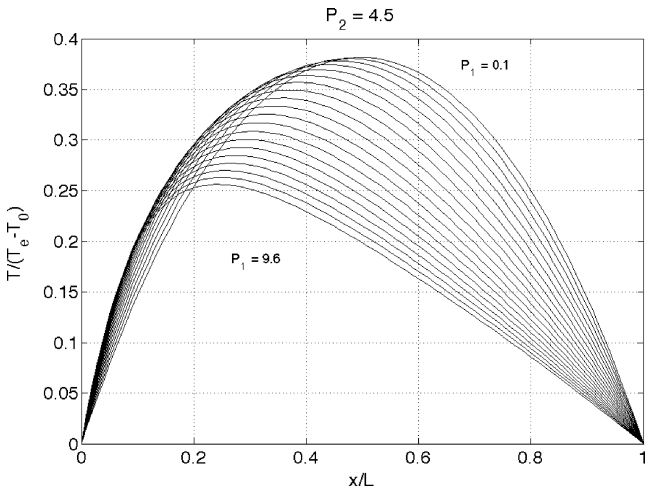

Fig. 13 Dimensionless temperature as computed by theory for $P_2=4.5$ and $0.1\leq P_1\leq 9.6$

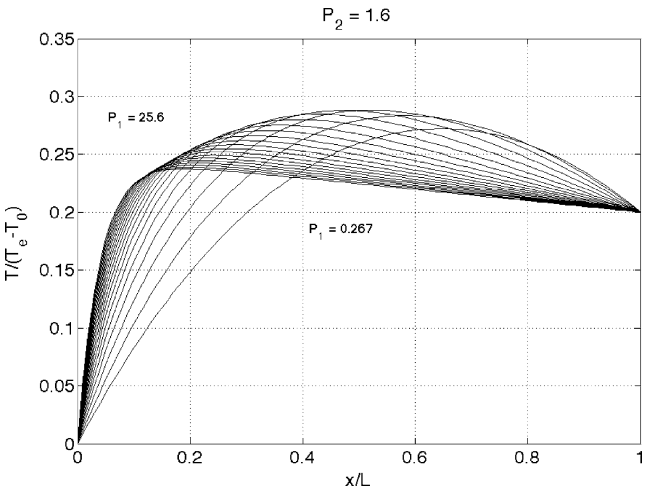

Fig. 15 The effects of flow for a case with asymmetrical boundary conditions: $\delta=0.2$, $P_2=1.6$, and $0.26\leq P_1\leq 25.6$

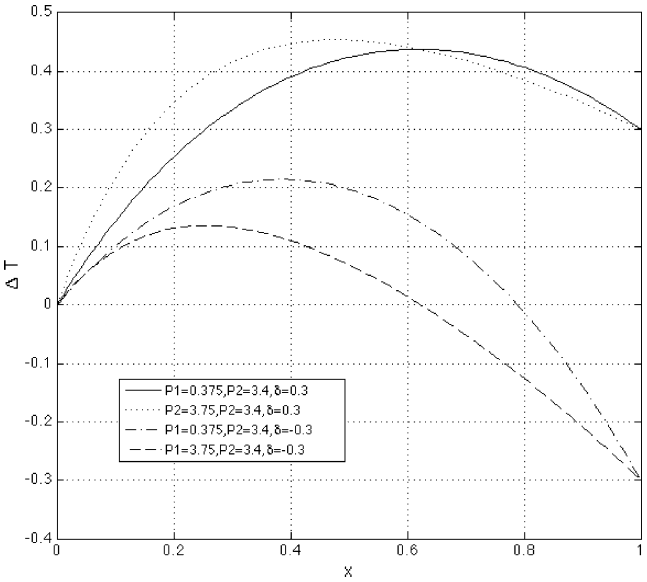

Fig. 16 Effect of upstream temperature condition and flow on temperature distributions

relatively cold; this should particularly be the case where selective withdrawal structure permits releases of cold hypolimnetic water (see e.g., Fischer et al. 1979). If we consider discharge from a reservoir, a distance L_{res} upstream of the tidal portion of the river at temperature T_{res}, and assume that dispersion is negligible in the river, then we find that the temperature rise coming from the reservoir to tidal river is

$$\Delta T_{\text{res-riv}} = (T_{\text{e}} - T_{\text{res}})\left(1 - \exp\left(\frac{-\alpha W L_{\text{res}}}{Q_f}\right)\right) \tag{17}$$

According to Eq. 17, the effect of increasing Q_f is most pronounced when Q_f is small. For example, for conditions typical of the San Joaquin, L_{res} (100 km), the change in temperature rise going from 5 to 20 $m^3\ s^{-1}$ is three times as large as the change for the same flow increment in going from 20 to 35 $m^3\ s^{-1}$. Likewise, the closer the reservoir is to the tidal river, the more closely the upstream temperature in the tidal river will reflect the reservoir release temperature.

Application of theory to observations

To apply this theory to the DWSC, it is necessary to estimate α, the heat transfer parameter. This can be done using the observations to compute T_{e} and then to use the observed surface heat transfer to compute α

$$\alpha = \frac{H_{\text{s}}}{\rho c_{\text{p}}(T_{\text{e}} - T_{\text{s}})} \tag{18}$$

T_{e} itself is calculated iteratively by computing heat flux as a function of water surface temperature (using the algorithms discussed above) and then finding the temperature at which the heat flux is zero. Calculated values of T_{e} for 2004 are shown in Fig. 17.

Using the value of α calculated from the data along with mean values of K (=600 m^2/s) and Q (=7.6 m^3/s) also calculated from the data, we find that $(P_1, P_2, \delta) = (0.49, 1.53, 0.37)$. Using these parameters, the predicted and measured dimensionless temperature distribution for 2004 are shown in Fig. 18. This comparison is quite encouraging, with the simple model representing both the spatial scale of the temperature variation and some rise in temperature in the DWSC. Alternatively, since α and Q are known, the theory can be used to estimate K and δ via non-linear fitting of the data to theory. Doing so using a non-linear, least squares regression method-based Gauss–Newton iteration (see e.g., Seber and Wild 2003), we find that the best fit values are K=607 m^2/s giving and δ=0.44. These give (P_1,P_2)=(0.49,1.53); the resulting distribution is also shown in Fig. 18.

The simple theory does not work nearly as well for 2005. As shown in Fig. 19, there is a significant difference between observations and theory. Most notably, the theory fails completely at predicting the elevated temperature in the interior. This is arguably an effect of unsteadiness in temperature during the 2005 experiment, a period of substantial cooling for which T_{e} dropped by 3°C over 2 weeks. Indeed, the interior dimensionless temperature initially appears to rise during the initial cooling phase, an effect of the fact that ΔT dropped much faster than the temperature field could actually adjust and then relaxes back to the steady solution, although given that the

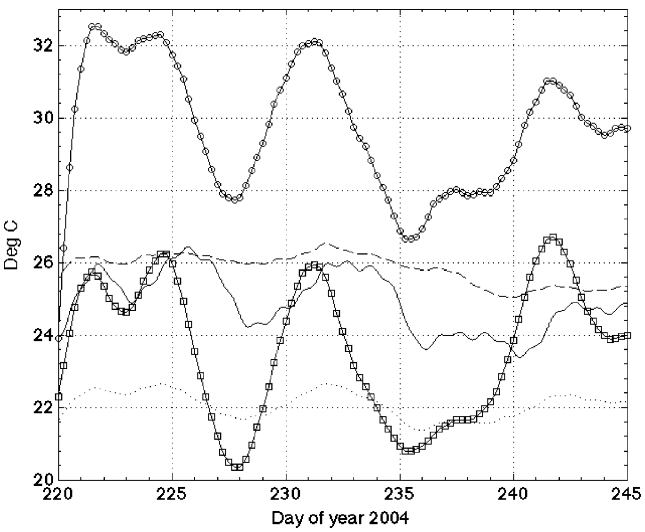

Fig. 17 Temperatures in San Joaquin DWSC in 2004: T_{e} (*circle*), T_{a} (*square*), and water temperatures at VER (*solid line*), M2 (*broken line*), and ANC (*dotted line*). All have been low pass filtered to remove diurnal variations

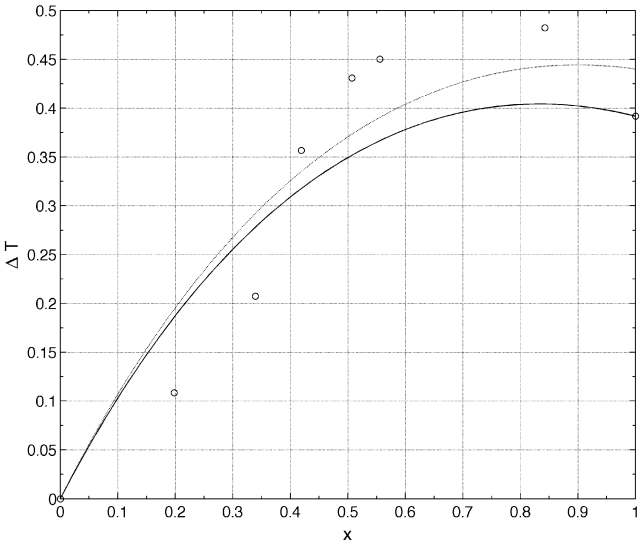

Fig. 18 Comparison of theory (*solid line*) with observations (*circle*) for 2004 conditions. Downstream boundary is set to PPT and upstream is set to MSD. Mean values from data are used for Q_f, K, and α. Observations are averages of temperatures between days 220 and 245. Theoretical curve based on best fit values of K and δ are also shown (*dotted line*)

adjustment time, which is O(LA/Q) (MacCready 1999), is approximately 30 days, this adjustment has not been completed by the end of the experiment. Thus, the 2005 data show that applicability of the simple theory is limited to times when the surface heat fluxes, or other forcing, are not rapidly changing, i.e., when $LA/Q \ll T_F$, where T_F is the timescale over which the forcing changes.

Discussion and Conclusions

Our observations and simple analytical model show that a balance of advection, dispersion, and surface forcing determines subtidal temperature variations in the DWSC, the tidal portion of the San Joaquin River. Notably, dispersion plays a significant role such that temperatures are elevated in the middle of the DWSC relative to both upstream riverine and downstream estuarine temperatures.

In examining the thermal energy balance for the DWSC, we used a very limited set of meteorological data, i.e., standard wind data (speed, direction, air temperature, and humidity) from one location and shortwave radiation data from another. This is likely appropriate for the domain that was the focus of our study. However, it may not be so for the larger issue of temperature prediction to meet temperature standards in the Delta. The reason is that the topography of the Delta leads to substantial variations in wind speeds along the length of the San Joaquin River and thus to variations in latent heat flux. In a like fashion, because of the diurnal movement of the marine cumulus layer (the fog)—significant variations in incident shortwave radiation, i.e., O(100 W m^2), might also be expected.

The thermal energy balance suggests a longitudinal dispersion coefficient, $K \approx 1{,}000$ m^2 s^{-1}, a value far in excess of what might be expected from existing descriptions of shear flow dispersion in rivers and estuaries, i.e., $K \approx 100$ m^2 s^{-1} or less (Fischer et al. 1979). Dispersion in the DWSC appears to result from a combination of how water parcels navigate the array of junctions and how flows in different connected channels are phased. In effect, this combination of processes may be considered to be a form of tidal pumping as described by Fischer et al. (1979), although given that multiple channels are involved also means that the dispersion may also have similarities to the chaotic dispersion model discussed by Ridderinkhof and Zimmerman (1992). Indeed, scale dependence should be expected since particle clouds that remain in a given channel only experience the kind of shear flow dispersion described by Eq. 7, whereas particle clouds that span a significant portion of the Delta effectively feel the dispersive effects of a number of channel junctions (Monsen 2001), leading (hypothetically) to the large dispersion coefficients we infer in this study.

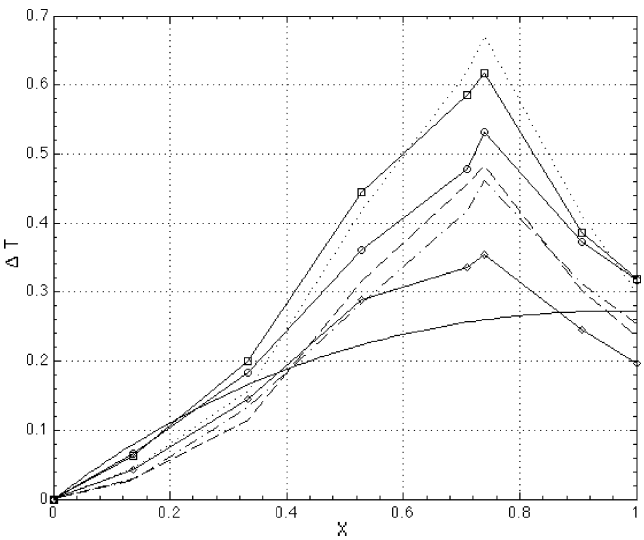

Fig. 19 Comparison of theory (*solid line*) with observations for 2005 conditions. For the theory, mean values from data are used for Q_f, K, and α. Longitudinal profiles at day 222.25 (broken wave tracings), day 224.75 (*dotted dashed line*), day 227.25 (*dotted line*), day 229.75 (*circle*), day 232.25 (*square*), and day 234.75 (*diamond*) have all been made dimensionless using values of T_e and T_0 appropriate to the time the profile represents. A single value is shown for the theory, since there was little variation in the dimensionless theoretical profile for this period

Acknowledgments The authors wish to thank the large group of students from Stanford and UC Davis as well as Jay Cuetara, John Yokimizo and their colleagues from the USGS California District, all of whom participated in the field work. This work was supported by CALFED Ecosystem Restoration Program contract ERP-02D-P51. SGM also is grateful for support from the Singapore Stanford Partnership.

Conflict of interest statement The authors have no financial relationship with the organization that sponsored the research. They also have no financial relationship with the publisher of *Estuaries and Coasts*. Finally, the authors have full control of all primary, data and they agree to allow the journal to review their data if requested.

References

Bennett, W.A. 2005. Critical assessment of the Delta Smelt population. *San Francisco Estuary and Watershed Science* 3(2), Article 1.

Bohrmans, M., and I.T. Webster. 1998. Dynamics of temperature stratification in lowland rivers. *ASCE Journal of Hydraulic Engineering* 12410: 1059–1063. doi:10.1061/(ASCE)0733-9429(1998)124:10(1059).

Cole, J.J., N.F. Caraco, and B.L. Peierls. 1992. Can phytoplankton maintain a positve carbon balance in a turbid, freshwater, tidal estuary? *Limnology and Oceanography* 37(8): 1608–1617.

DeGeorge, J.F. 1996. A multi-dimensional finite element transport model utilizing a characteristic-galerkin algorithm. Ph. D. Dissertation, University Of California, Davis.

Edinger, J.E., D.K. Brady, and J.C. Geyer. 1974. *Heat exchange and transport in the environment*. Electric Power Research Institute Report 14, 125 pp.

Fischer, H.B., E.J. List, R.C.Y. Koh, J. Imberger, and N.H. Brooks. 1979. *Mixing in Inland and coastal waters*. New York: Academic.

Fischer, H.B. 1976. Mixing and dispersion in estuaries. *Annual Review of Fluid Mechanics* 8: 107–133.

Jassby, A.D. 2005. Phytoplankton regulation in a eutrophic tidal river (San Joaquin River, California). *San Francisco Estuary and Watershed Science* 3(1), Article 3.

Jassby, A.D. and E.E. Van Nieuwenhuyse. 2005. Low dissolved oxygen in an estuarine channel (San Joaquin River, California): mechanisms and models based on long-term time series. *San Francisco Estuary and Watershed Science* 3(2), Article 2.

MacCready, P. 1999. Estuarine adjustment to changes in river flow and tidal mixing. *Journal of Physical Oceanography* 294: 708–726. doi:10.1175/1520-0485(1999)029<0708:EATCIR>2.0.CO;2.

Mohseni, O., and H.G. Stefan. 1999. Stream temperature/air temperature relationship: a physical interpretation. *Journal of Hydrology* 218: 128–141. doi:10.1016/S0022-1694(99)00034-7.

Monismith, S.G., W. Kimmerer, M.T. Stacey, and J.R. Burau. 2002. Structure and flow-induced variability of the subtidal salinity field in Northern San Francisco Bay. *Journal of Physical Oceanography* 32(11): 3003–3019.

Monsen, N.E. 2001. A study of sub-tidal transport in Suisun Bay and the Sacramento–San Joaquin Delta, California. PhD thesis. Stanford Univ.

Pawlowicz, R., B. Beardlsey, S. Lentz, E. Dever, and A. Anis. 2001. Software simplifies air–sea data estimates. *EOS Transactions of the American Geophysics Union* 82: 2. doi:10.1029/01EO00004.

Ridderinkhof, H., and J.T.F. Zimmerman. 1992. Chaotic stirring in a tidal system. *Science* 2585085: 1107–1109. doi:10.1126/science.258.5085.1107.

Romero, J.R., J.P. Antenucci, and J. Imberger. 2004. One- and three-dimensional biogeochemical simulations of two differing reservoirs. *Ecological Modeling* 174: 143–160. doi:10.1016/j.ecolmodel.2004.01.005.

Rueda, F.J., and S.G. Schladow. 2003. Dynamics of a large polymictic lake. II Numerical simulations. *Journal of Hydrologic Engineering* 1292: 92–101. doi:10.1061/(ASCE)0733-9429(2003)129:2(92).

Savenije, H.H.G. 2005. *Salinity and tides in alluvial estuaries*. Amsterdam: Elsevier.

Seber, G.A.F., and C.J. Wild. 2003. *Nonlinear regression*. New York: Wiley.

Tennekes, H., and J.L. Lumley. 1972. *A first course in turbulence*. Cambridge: MIT Press.

Uncles, R.J., and J.A. Stephens. 2001. The annual cycle of temperature in a temperate estuary and associated heat fluxes to the coastal zone. *Journal of Sea Research* 46: 143–159. doi:10.1016/S1385-1101(01)00078-8.